**Energy Proceedings**
Vol 35, 2023
ISSN 2004-2965

# Simulation study on the geological storage and transport of $CO_2$ in the saline aquifer

Guangda Ren[1], Yi Zhang [2*]

Key Laboratory of Ocean Energy Utilization and Energy Conservation Ministry of Education, School of Energy and Power Engineering, Dalian University of Technology, Dalian 116024, China.

(*Corresponding Author: Zhangyi80@dlut.edu.cn)

## ABSTRACT

With the rapid development of the global economy and the massive consumption of fossil energy, $CO_2$ emissions are increasing year by year, leading to global warming and triggering a series of ecological and environmental problems. Carbon capture and storage (CCS) technology is one of the most promising $CO_2$ emission reduction technologies. Subsurface storage of $CO_2$ in deep saline aquifer has received much attention due to its potential huge storage volume and technical feasibility. The large-scale implementation of $CO_2$ storage in saline aquifers is still confronted with complex reservoir structure, unclear spatial and temporal evolution of $CO_2$, and difficult to predict spatial spreading, and there is an urgent need to clarify the carbon migration behavior and influencing factors in the reservoir. In this paper, a simulation study of $CO_2$ storage in deep saline aquifer will be carried out in the Yaojia Formation of Sanzhao Depression in Songliao Basin. The 100-meter-deep sandstone stratum of the Yaojia Formation was selected for the study and divided into 10 lithologic layers, and the property parameters of each lithologic layer were assigned according to the actual situation. $CO_2$ was injected at a rate of 10kg/s for a total simulation time of 250 years, including 10 years of injection, and the stationary observation is 240 years. The results show that the density of supercritical $CO_2$ is slightly lower than that of water, and most of the $CO_2$ will float upward and a small amount of $CO_2$ will diffuse downward. After reaching the bottom of the cap layer, the $CO_2$ plume will migrate laterally along the cap layer. At the beginning of injection, most of the $CO_2$ will accumulate at the bottom of the cap, and a few will dissolve in the formation water. After injection stops, $CO_2$ has a tendency to continue to accumulate and migrate laterally to the cap layer. Over time, convection phenomena favoring $CO_2$ dissolution will occur.

**Keywords:** $CO_2$ geological sequestration； Deep saline aquifer； Numerical simulation

## 1. INTRODUCTION

Global climate change is increasing due to anthropogenic influences, and this phenomenon has been recognized by many countries. $CO_2$ is a major greenhouse gas, which is formed due to the massive consumption of fossil energy such as coal, oil and natural gas, so how to reduce $CO_2$ emissions is an urgent issue facing the world in the coming decades. Subsurface storage of $CO_2$ in deep saline aquifers has received much attention due to its potential application prospects and technical feasibility. In this paper, a simulation study of $CO_2$ storage in the deep saline aquifer will be conducted in the Yaojia Formation of Sanzhao Depression in Songliao Basin.

Several scholars in China and abroad have conducted research on geological storage of $CO_2$ in deep saline aquifers. Solomon[1] et al. constructed a complete three-dimensional axisymmetric $CO_2$ transport model and concluded that the saturation of liquid-phase $CO_2$ will increase by about 1% after $CO_2$ transport through the formation, mainly related to the salinity of the formation water[2, 3]. Pruess[4] et al. concluded that the effect of $CO_2$ sequestration tends to decrease with increasing vertical permeability. Ennis-King[5] et al. suggested that high vertical permeability is more beneficial to improve $CO_2$ sequestration. Ghanbari[6] et al. studied the dissolved sequestration of $CO_2$ in saline formations using STARTS simulator and concluded that dissolved sequestration is the dominant means of $CO_2$ sequestration and that the strong convective effect due to the dissolution of $CO_2$ during dissolved sequestration also leads to the capture of $CO_2$ during dissolved sequestration. Nicot[7] conducted a large-scale numerical simulation study of $CO_2$ injection in the Gulff-Coste Basin, Texas, USA, using Modflow96, and

---

# This is a paper for International CCUS Conference 2023 (ICCUSC2023), April 14-15, 2023, Beijing, China.

showed that over a 50-year period, with $CO_2$ injection at a rate of 0.5 Mt per year, the saline aquifer of the basin rose by about 1 m.

Based on the analysis of geological data of the Songliao Basin, it is tentatively concluded that the Sanzhao Depression is a more suitable site for $CO_2$ sequestration, in which the Yaojia Group formation can be considered as an ideal reservoir.

## 2 Numerical modeling of $CO_2$ sequestration in the saline aquifer

### *2.1 Introduction to the study area*

The Songliao Basin is home to the world's largest onshore oil and gas field, the Daqing Oilfield is one of the richest oil and gas regions in the world. The basin is rhombus-shaped, spanning Heilongjiang, Jilin, Liaoning and Inner Mongolia Autonomous Regions. The basin has a length of 750 km and a width of 330-370 km, covering an area of about 260,000 square kilometers.

First of all, in terms of geological factors, the Yaojia Formation can be sealed at depths of up to 1000-2000 m in some geological units, and $CO_2$ can exist in a supercritical form within a certain range. The upper part of the Yaojia Formation cover is mainly mudstone, which has good permeability and continuity, and its thickness also exceeds 200 m, which has strong confining ability. The stratigraphic thickness of the Yaojia Formation is in the range of 0-220 m. It has a high storage potential and is a site for longer-term and larger-scale $CO_2$ sequestration. There is no volcanic eruption around the Yaojia Formation in Sanzhao Depression, and the risk of geological disaster is low. Moreover, the $CO_2$ storage area in Sanzhao Depression is large and the distribution density of the waste well cluster is low, so its potential danger is very small in terms of $CO_2$ storage safety.

### *2.2 Model Building*

The Yaojia Formation of Sanzhao Depression in Songliao Basin was selected as the object of simulation study to establish a geological model close to the actual situation. The thickness of the Yaojia Formation is 0-210m, the depth is about 1300m, and the sandstone lithology is dominant. In this simulation study, the depth from the upper to the lower 100 meters is selected as the reservoir for simulation. The geological model is 140 m in the Z-direction, of which the upper 20 m is the cover and the lower 20 m is the basement cover, with a grid dissected every 10 m. The X-direction is 10,000 m, with 40 grids dissected, and the Y-direction is 5,000 m, with 20 grids dissected. The injection well is in the center with a length of 100 m. The total number of grids in the model is 11,200, and the specific model is shown in Figure 1.

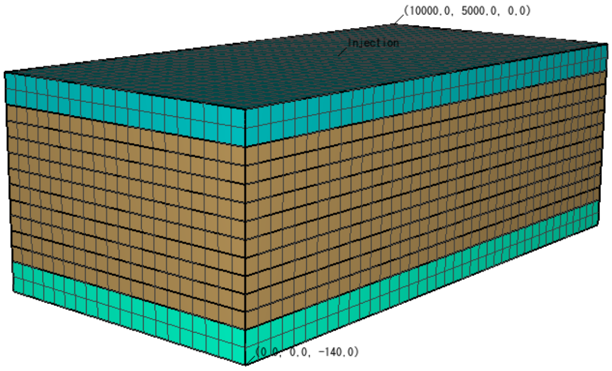

Fig. 1. Model View

The $CO_2$ injection point is 20 m away from the bottom of the reservoir, and the injection rate is 10 kg/s. The continuous injection is 10 years, and 240 years are observed after termination of injection, so the calculation period of the whole model is 250 years.

### *2.3 Model Parameters*

The porosity and permeability of the formations in the Songliao Basin are variable. According to Gao Ruiqi[8], who defined the relationship between sandstone porosity and depth in the study of oil and gas generation, transport and accumulation in the Yaojia Formation of the Songliao Basin, the relationship is as follows:

$$\phi = 0.4\exp(-0.5z) + 0.05$$

where $\phi$ is the porosity and Z is the stratigraphic depth (km).

In addition, the permeability of the rock body is also a critical parameter. The results show that the logarithmic value of permeability in the same type of rock mass is approximately linearly correlated with its pore coefficient, according to Xie Xignon[9] et al. on the high-pressure anomalous characteristics of the Tenaya Fault Trap in the Songliao Basin and the simulation study of fluid dynamics under different temperature and pressure conditions mentioned that:

$$K_x = 10^{22.58\phi - 18.15}$$

where $K_x$ denotes the permeability in the x-direction and ϕ is the porosity.

The permeability varies vertically and laterally in the rock mass and can be determined according to the following equation:

$$J = \frac{k_x}{k_z}$$

Where $J$ is the ratio of horizontal and vertical permeability and $k_z$ denotes the permeability in the vertical direction.

In this simulation, the 100 m formation was divided into 10 lithological layers, that is, the porosity and permeability of each lithological layer were the same, and the burial depth z was chosen as the center point height of each layer when performing the calculation. The values of porosity and permeability of each layer are shown in Table 1. In addition, an injection well with a diameter of 0.4 m was set up, and the characteristic parameters of the injection well are shown in Table 2. The initial pressure condition of the model is hydrostatic equilibrium pressure, and the temperature gradient is 3.8°C/100 m. The initial conditions of the injection point of the model are shown in Table 3. Except for the $CO_2$ inflow at the $CO_2$ injection point, the upper and lower boundaries and both boundaries are symmetric boundaries without mass flow

Tab. 1. Geological model lithological properties parameters calculation table

| Rock layer number | Z（m） | ϕ | Kx | J | Kz |
|---|---|---|---|---|---|
| cap layer | 1310 | 0.03 | 1.0E-16m$^2$ | 1 | 1.0E-16m$^2$ |
| 1 | 1325 | 0.258297 | 4.81E-13m$^2$ | 4 | 1.2E-13m$^2$ |
| 2 | 1335 | 0.257258 | 4.56E-13m$^2$ | 4 | 1.14E-13m$^2$ |
| 3 | 1345 | 0.256224 | 4.32E-13m$^2$ | 4 | 1.08E-13m$^2$ |
| 4 | 1355 | 0.255196 | 4.10E-13m$^2$ | 4 | 1.02E-13m$^2$ |
| 5 | 1365 | 0.254172 | 3.88E-13m$^2$ | 4 | 9.71E-14m$^2$ |
| 6 | 1375 | 0.253154 | 3.68E-13m$^2$ | 4 | 9.21E-14m$^2$ |
| 7 | 1385 | 0.252141 | 3.49E-13m$^2$ | 4 | 8.74E-14m$^2$ |
| 8 | 1395 | 0.251133 | 3.32E-13m$^2$ | 4 | 8.29E-14m$^2$ |
| 9 | 1405 | 0.250129 | 3.15E-13m$^2$ | 4 | 7.87E-14m$^2$ |
| 10 | 1415 | 0.249131 | 2.99E-13m$^2$ | 4 | 7.47E-14m$^2$ |

Tab. 2. Table of parameter values for injection wells

| Parameters | Density（kg/m$^3$） | ϕ | $k_x$ | Specific heat | Compression factor | Thermal conductivity |
|---|---|---|---|---|---|---|
| Injection well | 2600×10$^{40}$ | 0.3 | 10×10$^{-13}$ | 920 J/kg℃ | 4.5×10$^{-10}$Pa$^{-1}$ | 2.51W/m℃ |

Tab. 3. Model injection point initial conditions

| Injection speed | Injection time | Temperature | Pressure | Salinity |
|---|---|---|---|---|
| 10kg/s | 10years | 333.15K | 135bar | 0.40％ |

TOUGH2 provides a total of eight models available for the relative permeability coefficient and capillary pressure models. By default, the Van Genuchten-Mualem and Corey functions are used for the relative permeability coefficient model, and the Van Genuchten model is used for the capillary pressure model, as shown in the following functional forms.

Relative permeability coefficient model (liquid phase - Van Genuchten):

$$k_{rl} = \sqrt{S^*}\{1-(1-[S^*]^{1/m})^m\}^2$$

$$S^* = \frac{S_l - S_{lr}}{1 - S_{lr}}$$

Where $k_{rl}$ denotes the relative permeability coefficient of the liquid phase, $S_l$ denotes the liquid phase saturation, residual liquid saturation $S_{lr}$=0.30, and exponent m=0.457.

Relative permeability coefficient model (gas-phase-Corey):

$$k_{rg} = (1-\hat{S})^2(1-\hat{S}^2)$$

$$\hat{S} = \frac{S_l - S_{lr}}{S_l - S_{lr} - S_{gr}}$$

where $k_{rg}$ denotes the relative permeability coefficient of the gas phase and the residual gas saturation $S_{gr}$=0.05.

Capillary pressure model (Van Genuchten):

$$P_{cap} = -P_0([S^*]^{-1/m}-1)^{1-m}$$

$$S^* = \frac{S_l - S_{lr}}{1 - S_{lr}}$$

Where $P_{cap}$ denotes capillary pressure, residual liquid saturation $S_{lr}$=0, m=0.457, and concentration factor $P_0$=19.61kpa.

### 2.4 Model Results

The distribution of $CO_2$ gas saturation at different times and the amount of $CO_2$ sequestration at different states are monitored by numerical simulation.

#### 2.4.1 Injection period

The variation of $CO_2$ gas saturation during the injection period is shown in figure 2-figure supplement 4. The $CO_2$ storage capacity is shown in Table 4.

During the $CO_2$ injection process, the following conclusions were drawn: As can be seen from figure 2, during the injection stage, the injected $CO_2$ migrates upward under buoyancy because the density of supercritical state $CO_2$ is smaller than water, and the saturation of gas-phase $CO_2$ in the pore space gradually increases. After about 120 days, $CO_2$ reaches the bottom of the cap layer, and $CO_2$ starts to migrate along the bottom by lateral diffusion under the blockage of the cap layer. At the termination of gas injection, $CO_2$ accumulates 81% at 10 meters from the upper cap layer and 88% at 20 meters from the upper cap layer. $CO_2$ uplift and lateral transport have a certain regularity, which has high requirements on the stability of the cap layer, and the lower permeability, larger thickness and better continuity of the cap layer are more favorable for $CO_2$ sequestration.

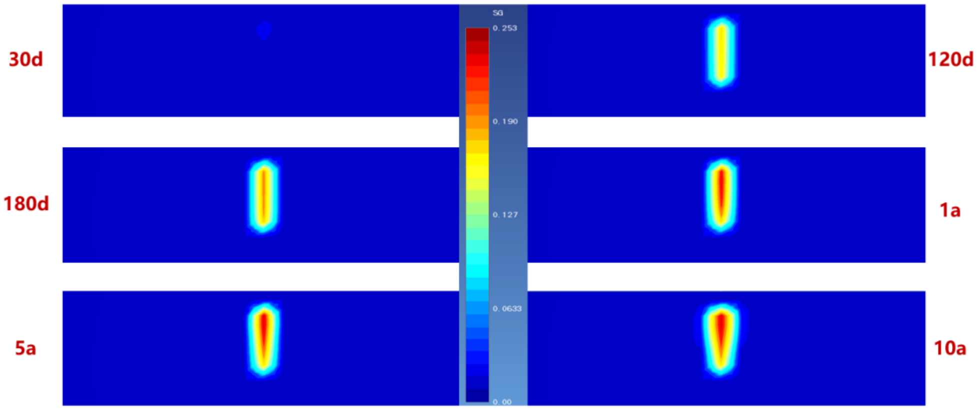

Fig. 2. Cloud map of $CO_2$ gas saturation during injection

From figure 3, it can be seen that due to the effect of vertical permeability, the vast majority of the injected $CO_2$ dissolves in the formation water along the injection well before 30 days, when the peak $CO_2$ gas saturation is 0.001. At 120 days the peak $CO_2$ gas saturation rises to 0.17. After one year, the $CO_2$ gas saturation reaches the maximum value of 0.23 during the injection period, and with the passage of time, the The $CO_2$ gas saturation decreases slightly over time because the rate of $CO_2$ diffusion downward is slightly greater than the rate of $CO_2$ migration upward. 605 m of $CO_2$ is migrated to both sides after 5 years. After 10 years, the migration distance is about 752 m.

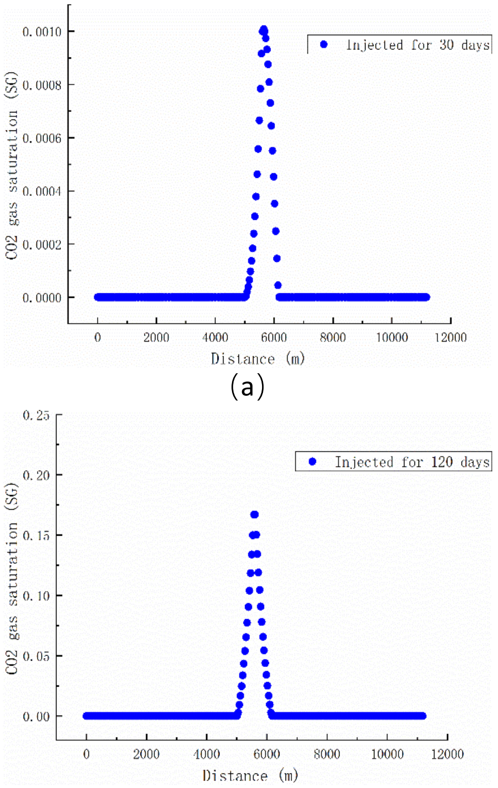

(a)

(b)

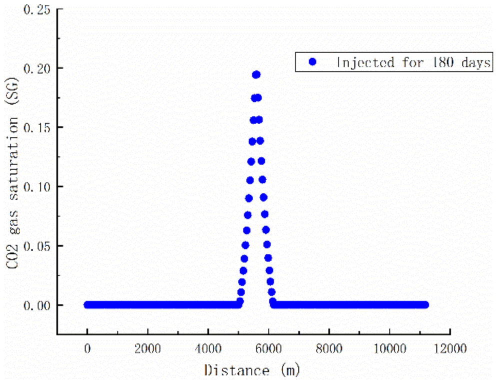

(c)

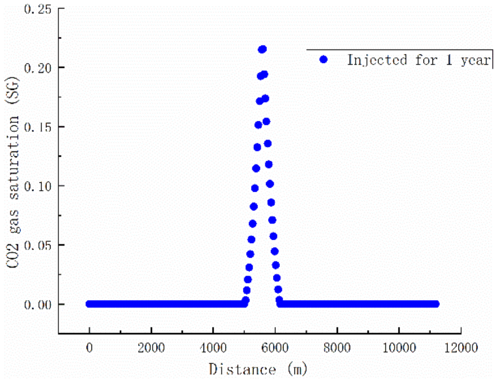

(d)

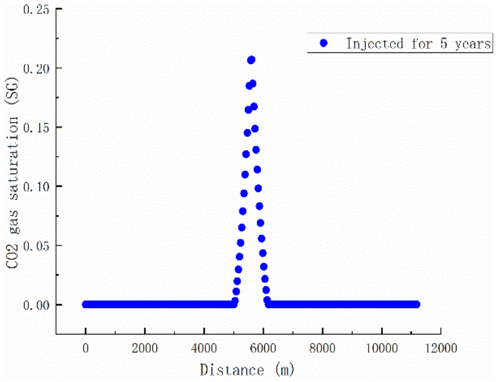

(e)

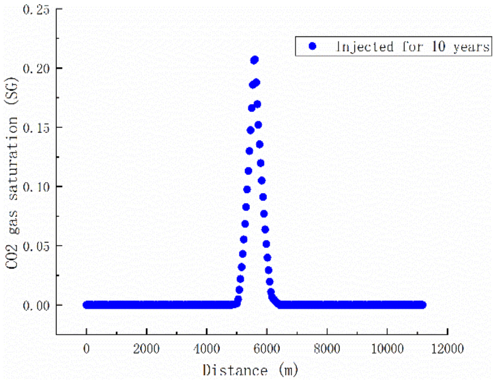

(f)

Fig. 3. Variation of $CO_2$ gas saturation with distance during injection

As can be seen from Table 4, the fraction of the mass of $CO_2$ dissolved in formation water to the total storage during the injection period ranged from 25% to 34.39%, and the mass of $CO_2$ dissolved in formation water accounted for less and less of the total sequestered $CO_2$ mass as time increased, indicating that $CO_2$ existed mainly in the gaseous (supercritical) form, with a small amount dissolved in formation water, and the gas phase sequestration rate is larger than the dissolved sequestration rate. On day 1, there are $2.97\times10^5$ kg of $CO_2$ dissolved in the formation water and $5.66\times10^5$kg in the free gaseous state. In year 10, there are $7.87\times10^8$ kg of $CO_2$ dissolved in the formation water and $2.36\times10^9$ kg in the free gaseous state.

Tab. 4. $CO_2$ sequestration during injection

| Times | Gas phase（kg） | Liquid phase（kg） | Total（kg） |
|---|---|---|---|
| 1day | 5.6651E+05 | 2.9694E+05 | 8.6345E+05 |
| 30 days | 1.7813E+07 | 8.0703E+06 | 2.5883E+07 |
| 60 days | 3.5673E+07 | 1.6095E+07 | 5.1768E+07 |
| 100 days | 5.8844E+07 | 2.7501E+07 | 8.6345E+07 |
| 120 days | 7.1535E+07 | 3.2395E+07 | 1.0393E+08 |
| 180 days | 1.0280E+08 | 5.3099E+07 | 1.5590E+08 |
| 1 year | 2.1086E+08 | 1.0395E+08 | 3.1481E+08 |
| 5 years | 1.1530E+09 | 4.2601E+08 | 1.5790E+09 |
| 8 years | 1.8664E+09 | 6.5201E+08 | 2.5184E+09 |
| 10 years | 2.3611E+09 | 7.8703E+08 | 3.1481E+09 |

It can be seen from figure 4 that the slope of $CO_2$ gas phase sequestration is significantly higher than that of liquid phase sequestration, which can also indicate that $CO_2$ exists mainly in gaseous form, with a small amount dissolved in the formation water, and the upward migration rate is larger than the dissolution rate.

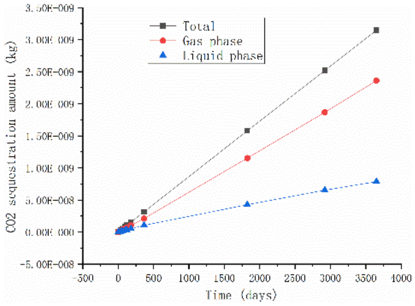

Fig. 4. $CO_2$ sequestration during injection

### 2.4.2 Changes between cessation of injection and 250 years

After the injection was stopped, $CO_2$ continued to diffuse outward. Figures 5-figure 7 show the variation of $CO_2$ gas saturation. The $CO_2$ storage is shown in Table 5.

The main conclusions obtained were as follows: From figure 5, it can be seen that the $CO_2$ gas saturation is decreasing year by year after the cessation of injection. Due to the multiple effects of gravity, concentration gradient and buoyancy, $CO_2$ is further dissolved in formation water, forming dissolved sequestration, which is because the rate of $CO_2$ diffusion into formation water is greater than the rate of $CO_2$ upward and lateral migration. More and more gaseous $CO_2$ in the reservoir dissolves in the formation water as time goes by. However, within 50 years, the amount of gaseous (supercritical) $CO_2$ is still much greater than the amount of $CO_2$ dissolved in formation water.

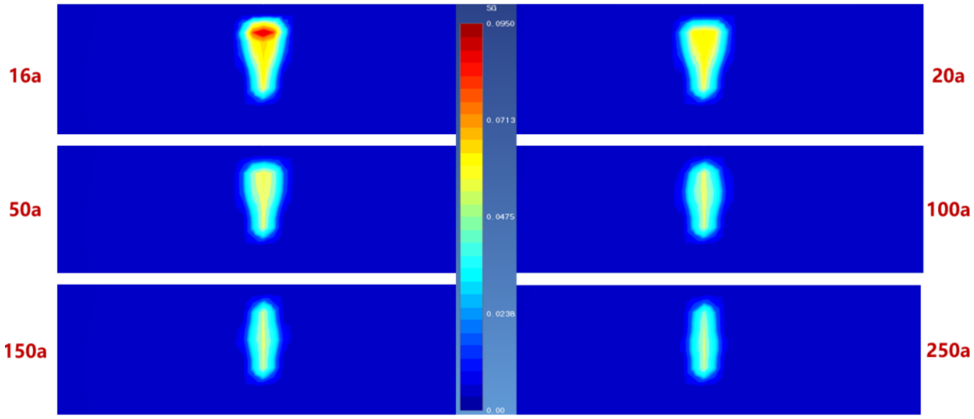

Fig. 5. Cloud map of $CO_2$ gas saturation after stopping injection

From figure 6, it can be seen that the $CO_2$ gas saturation corresponding to different moments after stopping injection varies with distance. The $CO_2$ saturation in the supercritical state varies between 0.05 and 0.065. The $CO_2$ gas saturation reaches a maximum of 0.065 at about 16 years. After that, the $CO_2$ gas saturation no longer increases and decreases as time advances. As the distance from the injection well increases, the The $CO_2$ gas saturation also decreases as the distance from the injection well increases. In years 50 and 100, $CO_2$ migrates about 875 m and 1050 m to both sides of the injection well. In year 250, the $CO_2$ gas saturation decreases to 0.05 and $CO_2$ migrates a total of 1350 m to both sides of the injection well.

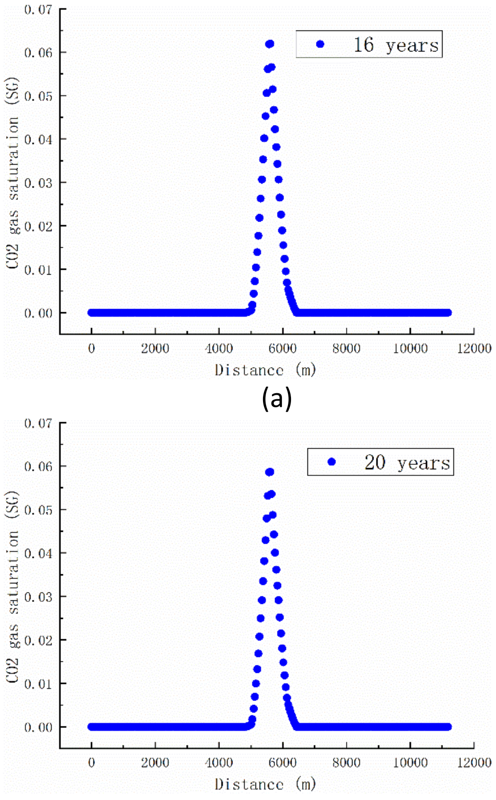

(a)

(b)

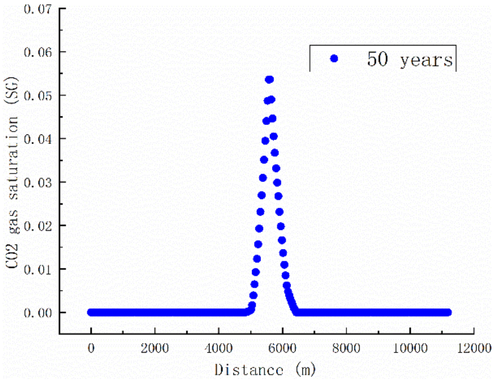

(c)

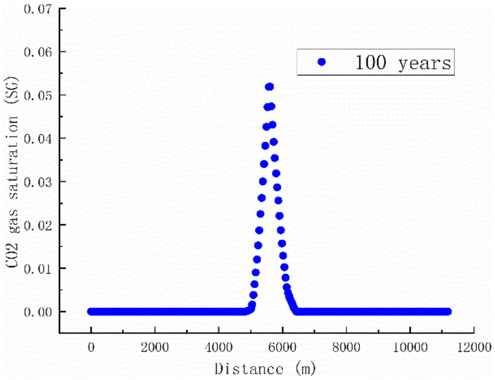

(d)

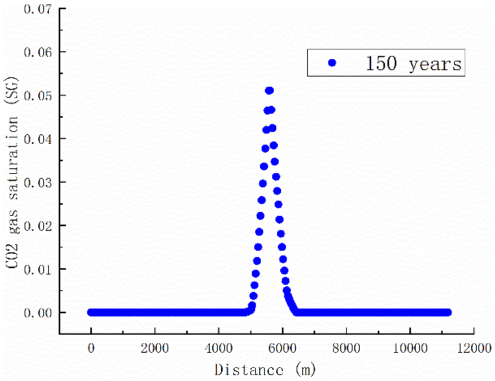

(e)

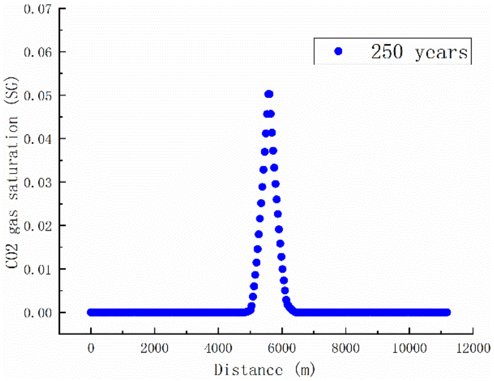

(f)

Fig. 6. Plot of $CO_2$ gas saturation with distance when injected and stopped

From the $CO_2$ storage volume after the cessation of injection in Table 5, it can be seen that in the 20th year, the mass of gas-phase $CO_2$ is $2.04\times10^9$ kg and the mass of liquid-phase $CO_2$ is $1.11\times10^9$ kg, and 35.31% of the injected $CO_2$ is dissolved in the formation water. In 100 years, the mass of gas-phase $CO_2$ is $1.66\times10^9$ kg and the mass of liquid-phase $CO_2$ is $1.49\times10^9$ kg. At 180 years, about half of the $CO_2$ was dissolved in the formation water. And at 200 years, the proportion of injected $CO_2$ dissolved in the formation water had exceeded 50%, reaching 50.87%. At 250 years, the dissolved amount reached 52.53%.

Tab. 5. $CO_2$ sequestration status

| Times | Gas phase （kg） | Liquid phase （kg） | Total （kg） | Percentage of liquid phase |
|---|---|---|---|---|
| 20 years | 2.0363E+09 | 1.1115E+09 | 3.1478E+09 | 35.31％ |
| 40 years | 1.9617E+09 | 1.1861E+09 | 3.1478E+09 | 37.68％ |
| 50 years | 1.9053E+09 | 1.2425E+09 | 3.1478E+09 | 39.47％ |
| 90 years | 1.6749E+09 | 1.4729E+09 | 3.1478E+09 | 46.79％ |
| 100 years | 1.6560E+09 | 1.4918E+09 | 3.1478E+09 | 47.39％ |
| 125 years | 1.6255E+09 | 1.5223E+09 | 3.1478E+09 | 48.36％ |
| 160 years | 1.5899E+09 | 1.5579E+09 | 3.1478E+09 | 49.49％ |
| 200 years | 1.5465E+09 | 1.6013E+09 | 3.1478E+09 | 50.87％ |
| 220 years | 1.5273E+09 | 1.6205E+09 | 3.1478E+09 | 51.48％ |
| 240 years | 1.5068E+09 | 1.6410E+09 | 3.1478E+09 | 52.13％ |
| 250 years | 1.4942E+09 | 1.6536E+09 | 3.1478E+09 | 52.53％ |

As can be seen from the slope of the curves of gas-phase and liquid-phase $CO_2$ storage in Figure 7, a significant convection phenomenon occurs around 50 years. This is caused by $CO_2$ dissolving in saline aquifer and increasing its density, moving downward under the effect of gravity. This convective effect promotes the dissolution rate and spatial distribution range of $CO_2$, increasing the effective storage of $CO_2$ and the security of long-term storage. Both structural and dissolved storage are mainly considered, so the total storage volume remains constant, and the gas-phase storage volume is gradually decreasing after the cessation of injection, while the liquid-phase storage volume is gradually increasing, and the dissolved storage volume exceeds the structural storage volume at 180 years.

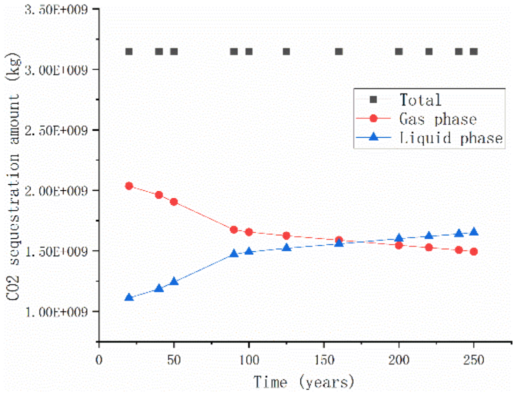

Fig. 7. Amount of $CO_2$ sequestered after injection has stopped

## 3. Conclusions

(1) Injection period: Because the density of $CO_2$ is less than water in the supercritical state, most of the $CO_2$ will migrate upward with the injection well, and a small amount of $CO_2$ will diffuse downward. Due to the effect of vertical permeability, most of the injected $CO_2$ is dissolved in the formation water along the injection well before 30 days. After about 120 days, $CO_2$ reaches the bottom of the cap layer, and $CO_2$ is transported laterally under the blockage of the cap layer. After one year, the $CO_2$ gas saturation reaches the maximum value of 0.23 during the injection period and decreases slightly with time. At the end of injection, $7.87\times10^8$ kg of $CO_2$ is dissolved in formation water, $2.36\times10^9$ kg of $CO_2$ is in free gas state, and about 25% of $CO_2$ is dissolved in formation water. At the end of the 10th year of gas injection, 81% of $CO_2$ was accumulated at 10 meters from the upper cover layer and 88% at 20 meters from the upper cover layer.

(2) After the cessation of injection: $CO_2$ further diffuses into the formation water under the effect of gravity, and the proportion of liquid-phase $CO_2$ becomes higher and higher. In the 20th year, 35.31% of the injected $CO_2$ is dissolved in the formation water, and the $CO_2$ storage volume after the cessation of injection shows that the mass of gas-phase $CO_2$ is $2.04\times10^9$ kg and the mass of liquid-phase $CO_2$ is $1.11\times10^9$ kg. The slope of the curve shows that after 50 years, there is an obvious convection phenomenon. This is due to $CO_2$ dissolving in saline water and increasing its density, moving downward under the effect of gravity. This convective action promotes the contact between $CO_2$ and formation water and facilitates the convective diffusion of $CO_2$. At 100 years, the mass of $CO_2$ in the gas phase is $1.66\times10^9$ kg and the mass of $CO_2$ in the liquid phase is $1.49\times10^9$ kg. At 185 years, about half of the $CO_2$ is dissolved in formation water. And at the 200th year, the proportion of the injected $CO_2$ dissolved in formation water has exceeded 50% and It reached 50.87%. At 250 years, the $CO_2$ migrated to both sides of the injection well for a total of 1350 meters.

## DECLARATION OF INTEREST STATEMENT

The authors declare that they have no known competing financial interests or personal relationships that could have appeared to influence the work reported in this paper. All authors read and approved the final manuscript.

## REFERENCE

[1] Solomon S, Carpenter M, Flach T A. Intermediate storage of carbon dioxide in geological formations: A technical perspective[J]. INTERNATIONAL JOURNAL OF GREENHOUSE GAS CONTROL. 2008, 2(4): 502-510.

[2] Enick R M, Klara S M. $CO_2$ SOLUBILITY IN WATER AND BRINE UNDER RESERVOIR CONDITIONS[J]. CHEMICAL ENGINEERING COMMUNICATIONS. 1990, 90: 23-33.

[3] Bachu S, Adams J J. Sequestration of $CO_2$ in geological media in response to climate change: capacity of deep saline aquifers to sequester $CO_2$ in solution[J]. ENERGY CONVERSION AND MANAGEMENT. 2003, 44(20): 3151-3175.

[4] Pruess K, Xu T F, Apps J, et al. Numerical Modeling of aquifer disposal of $CO_2$[J]. SPE JOURNAL. 2003, 8(1): 49-60.

[5] Ennis-King J, Paterson L. Role of convective mixing in the long-term storage of carbon dioxide in deep saline formations[J]. SPE JOURNAL. 2005, 10(3): 349-356.

[6] Ghanbari S, Al-Zaabi Y, Pickup G E, et al. Simulation of $CO_2$ storage in saline aquifers[J]. CHEMICAL ENGINEERING RESEARCH & DESIGN. 2006, 84(A9): 764-775.

[7] Nicot J P. Evaluation of large-scale $CO_2$ storage on fresh-water sections of aquifers: An example from the Texas Gulf Coast Basin[J]. International Journal of Greenhouse Gas Control. 2008, 2(4): 582-593.

[8] Yang W. L., Gao R. K., Guo Q. F., et al. Onshore oil and gas generation, transport and accumulation in the Songliao Basin [M]. The Generation, Transport and

Aggregation of Onshore Oil and Gas in the Songliao Basin, 1985.
[9] Xie X. N., Jiao J. J., Xiong H. H. Anomalous low-pressure system and its genesis mechanism in the Ten House Fault in the Songliao Basin[J]. Earth Science: Journal of China University of Geosciences. 2003, 28(1): 61-66.